MEaSUREs Grounding Zone of the Antarctic Ice Sheet, Version 1

USER GUIDE

How to Cite These Data

As a condition of using these data, you must include a citation:

Rignot, E., J. Mouginot, and B. Scheuchl. 2022. *MEaSUREs Grounding Zone of the Antarctic Ice Sheet, Version 1*. [Indicate subset used]. Boulder, Colorado USA. NASA National Snow and Ice Data Center Distributed Active Archive Center. https://doi.org/10.5067/HGLT8XB480E4. [Date Accessed].

FOR QUESTIONS ABOUT THESE DATA, CONTACT NSIDC@NSIDC.ORG

FOR CURRENT INFORMATION, VISIT https://nsidc.org/data/NSIDC-0778

National Snow and Ice Data Center

TABLE OF CONTENTS

1 DATA DESCRIPTION

This data set provides a comprehensive map for the Antarctic Ice Sheet of the short-term zone of migration of the grounding line (i.e., the transition boundary between grounded ice and ice floating in the ocean waters) over a given period due to changes in oceanic tide. This short-term variation in the grounding line is referred to in this data set as the "grounding zone." The grounding zone is presented as polylines in an ESRI shapefile indicating the upstream and downstream bound of the variation in the grounding line for a given year. The data is based on an automatic delineation of thousands of grounding lines using Sentinel-1 A/B interferometric synthetic aperture radar (InSAR) data with a machine learning algorithm and supplemented by grounding lines from COSMO SkyMed InSAR data.

1.1 Parameters

This data set provides the upstream and downstream boundary of the grounding zone for ice sheets. It provides a single boundary for islands (i.e., areas of emergent land where ice is grounded) and ephemeral ice rises (i.e., areas where the ice shelf is in contact with the seafloor only during a part of the tidal cycle).

1.2 File Information

1.2.1 Format

The data file is provided as an ESRI shapefile (`.shp`, `.shx`, `.dbf`, `.cpg`, `.prj`, and `.qpj`).

1.2.2 File Contents

Table 1 describes the parameters that are included in `Antarctic_GZ_2018_v01.0.shp`.

Table 1. Parameter Details

Parameter	Description	Values
Name	Glacier or ice shelf name	Name
Sensor	Sensor used to determine the grounding zone	CSK = COSMO SkyMed S1 = Sentinel-1 SAR Interferometric Wide swath mode (IW) CSK S1 = COSMO SkyMed and Sentinel-1 SAR IW
Year	4-digit year represented by grounding zone	2018, 2019, or 2020

Type	Type of ice feature	Ice Sheet, Ephemeral Ice Rise (EIR), or Island
Boundary	For ice sheets, this parameter indicates if the polyline denotes the upper or lower boundary of the grounding zone. For EIRs and islands only one boundary is provided.	Up or Dn (Down)
ID_IS	For ice sheets, this parameter is a numerical ID used to differentiate between the polylines denoting the upper and lower boundaries. For EIR and islands this is set to 200 as there is only one boundary.	1-200
ID	Unique numerical ID assigned to each record	1-264

1.2.3   Naming Convention

The data set includes one shapefile, `Antarctic_GZ_2018_v01.0.xxx`, named according to convention described in Table 2.

Table 2. File Naming Convention

Variable	Description
Antarctic	Geographic location
GZ	Grounding zone
2018	Primary year of SAR data acquisition
v01.0	Data set version
.xxx	File type (`.shp`, `.shx`, `.dbf`, `.cpg`, `.prj`, and `.qpj`)

1.3 Spatial Information

1.3.1   Coverage

The data set spans the Antarctic Ice Sheet:

- Southernmost Latitude: 90° S
- Northernmost Latitude: 60° S
- Easternmost Longitude: 180° W
- Westernmost Longitude: 180° E

1.3.2   Resolution

The interferometric SAR data underlying this product are posted at 100 m.

1.3.3   Geolocation

The following tables provide information for geolocating this data set.

Table 3. Geolocation Details

Geographic coordinate system	WGS 84
Projected coordinate system	WGS 84 / Antarctic Polar Stereographic
Longitude of true origin	0
Latitude of true origin	-71
Scale factor at longitude of true origin	1
Datum	WGS_1984
Ellipsoid/spheroid	WGS 84
Units	meter
False easting	0
False northing	0
EPSG code	3031
PROJ4 string	+proj=stere +lat_0=-90 +lat_ts=-71 +lon_0=0 +k=1 +x_0=0 +y_0=0 +datum=WGS84 +units=m +no_defs
Reference	https://epsg.io/3031

1.4 Temporal Information

1.4.1   Coverage

The data represents grounding zones for 2018, 2019, or 2020, depending on imagery availability.

This product complements the delineation of grounding lines for 1992-2014 provided in MEaSUREs Antarctic Grounding Line from Differential Satellite Radar Interferometry.

2   DATA ACQUISITION AND PROCESSING

2.1 Acquisition

This data set was produced with Sentinel-1 A/B and COSMO SkyMed synthetic aperture radar (SAR) data using the differential satellite interferometric synthetic aperture radar (DInSAR) technique. DInSAR provides a measurement of the short-term variability in ice motion by differencing two temporally consecutive radar interferograms spanning the same spatial interval. The interferometric measurement is sensitive to different tide levels and subsequent vertical ice motion, or flexes, when the images were taken. As the grounding line is associated with ice flexes,

this allows for grounding line detection (Figure 1). DInSAR is the most precise and efficient method for delineating grounding lines, with the ability to detect ice motion within millimeter precision.
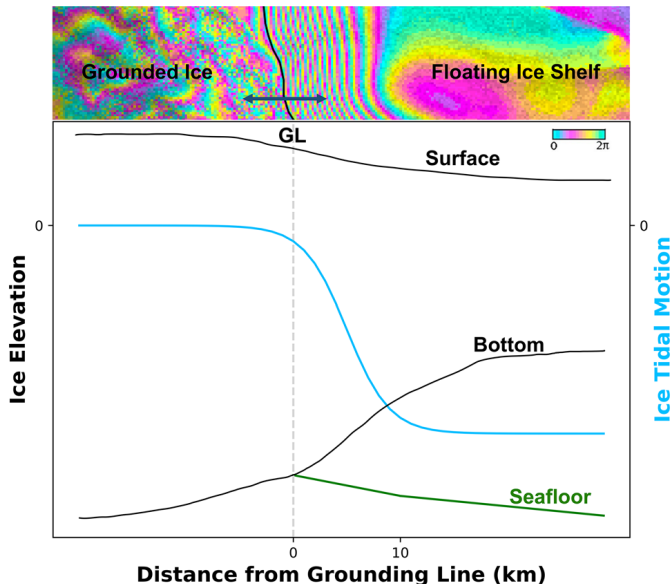

Figure 1. Schematic of the ice surface, ice bottom elevation, sea floor depth, and vertical tidal motion of the ice in the grounding zone versus a differential SAR interferogram on top. The grounding line, represented by the vertical gray dashed line, is at the inner most fringe of the grounded ice side. The differential motion in the tidal flexing zone produces a dense fringe pattern used by the machine learning model to identify grounding lines. The direction of horizontal migration of the grounding line is shown by the double sided dark blue arrow. Source: Mohajerani, 2021.

2.2 Processing

The data is based on an automatic delineation of thousands of grounding lines using Sentinel-1A/B InSAR data and a machine learning algorithm that employs a fully convolutional neural network. The data is supplemented by manually drawn grounding lines from the COSMO SkyMed constellation in several areas. A detailed description is given below and in Mohajerani et al. (2021).

2.2.1   DInSAR Data

To streamline computation, all DInSAR interferogram input images were split into 512 x 512 pixel tiles, with each pixel representing 100 m x 100 m. The model output has the same dimensions. Larger scenes were reconstructed by stitching tiles using a Gaussian averaging filter. As a form of data augmentation and to avoid edge effects, tiles partially overlapped in four directions and were on a staggered grid, producing eight partial coverings of each area.

2.2.2 Training and Testing

To create training and testing data sets for the model, grounding lines were manually delineated and rasterized for a total of 252 DInSAR-delineation pairs, split into 5,320 tiles, from Sentinel-1 A/B data for the Getz Ice Shelf. A batch size of 30 tiles was used and the data were trained over nine approximately 10 minute epochs, chosen based on a minimum improvement threshold to avoid overfitting. Once training was complete, the network was tested on 500 tiles. The input data, the manual training labels, and output of the neural network are shown in Figure 2.
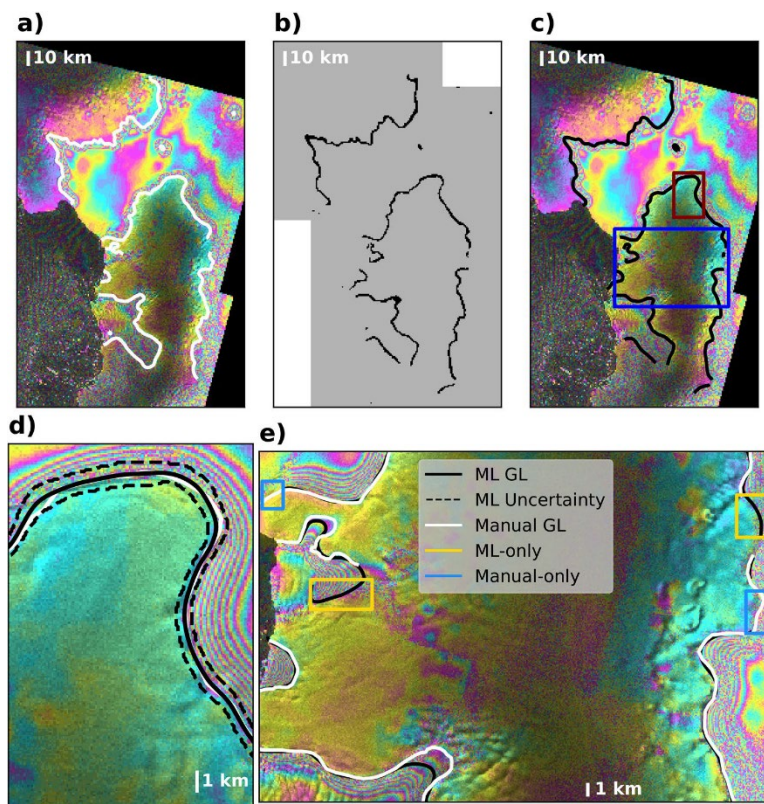

Figure 2. Different steps of the analysis for (a) a sample interferogram with manually drawn grounding line in white; (b) output of the neural network in raster format with a variable width corresponding to the uncertainty of the output. The gray mask in the background represents training (white) and testing (gray) sites; (c) vectorized output and uncertainty contours; (d) zoomed-in region highlighted by the maroon box in panel (c) showing both manual and machine learning results and uncertainty bars; (e) comparison of the manual and machine learning performances in the area outlined in blue in panel (c). Source: Mohajerani, 2021.

2.2.3 Output

After training and testing, the model was run to delineate grounding lines on 22,935 DInSAR interferograms over Antarctica. The output raster represented the probability of each pixel belonging to the grounding line. To vectorize the raster output, closed contours were drawn around grounding line pixels using a probability distribution threshold of 30% (e.g., the probability of a pixel

belonging to the grounding line class) to represent uncertainty (Figure 2d). The width of the contours represents the uncertainty estimate of the neural network output. The grounding line was determined by automatically drawing a centerline between these uncertainty estimates, which comprises the final output product.

2.2.4 Model Details

The machine learning model includes a 40-layer deep encoder-decoder convolutional neural network with parallel atrous convolutional layers (Atrous Spatial Pyramid Pooling), resembling the DeepLabv3+ architecture. Depthwise separable convolutions for parallel atrous layers are used to minimize the number of trainable parameters. Skip connections between encoding and decoding layers are used to convey contextual information. All convolutional layers use the Exponential Linear Unit (ELU) activation function, with the exception of the last convolutional layer, which uses a sigmoid activation function producing the predicted probability of the class of each pixel. In total, 966,119 trainable parameters are used in the model. To account for the large class imbalance between non-grounding-line to grounding-line pixels, a weighted binary cross entropy loss function is used to penalize false negatives more harshly than false positives.

2.3 Quality, Errors, and Limitations

The length of the vectorized output grounding lines was used to filter noisy outputs, with a threshold of 6 km set to eliminate small features while avoiding exclusion of real features. To quantify confidence in the machine learning model performance, manual delineation was performed on grounding lines not used during training and the mean difference between the neural-network and manual-grounding line was calculated. The mean difference was found to be 232 m (2.3 pixels) with a median absolute deviation of 101 m and interquartile range of 131 m, indicating that the machine learning algorithm performs comparably to manual delineation. The machine learning approach also offers an advantage over manual delineation by providing uncertainty bounds. The mean uncertainty was found to be 451 m (4.5 pixels), with a range of 151 m to 1,427 m in high noise scenarios.

The Sentinel-1 A/B model derived data is supplemented by manually drawn grounding lines from COSMO SkyMed data in several areas, including the Amundsen Sea Embayment sector of West Antarctica (Pine Island, Thwaites, Haynes, Pope, Smith, and Kohler glaciers), and Denman and Totten glaciers in East Antarctica.

2.4 Instrumentation

Table 4 lists the parameters for each satellite sensor used in this data set. For more information, see the Italian Space Agency COSMO-SkyMed and European Space Agency Copernicus Sentinel-1 websites.

Table 4. Parameters of Source Satellite Data

Parameter	COSMO SkyMed	Sentinel-1
Repeat Cycle	16-day	12-day for individual satellites; 6-day for both
Band	X-Band	C-Band
Mode	Himage Polarimetric	Interferometric Wide
Incidence Angle	40.3°	32.3°
Number of Range Looks (Interferogram)	10	20
Number of Azimuth Looks (Interferogram)	10	2
Range pixel spacing (resolution)	3 (<3 m)	3 (2.3 m)
Azimuth pixel spacing (resolution)	3 (<3 m)	22(17.4 m)

3   SOFTWARE AND TOOLS

The algorithm, model configuration, and trained model used to create this data set can be accessed at the following GitHub repository: https://github.com/yaramohajerani/GL_learning.

4   RELATED DATA SETS

MEaSUREs Data at NSIDC

MEaSUREs Antarctic Grounding Line from Differential Satellite Radar Interferometry

5   REFERENCES

Mohajerani, Y., Jeong, S., Scheuchl, B., Velicogna, I., Rignot, E., & Milillo, P. (2021). Automatic delineation of glacier grounding lines in differential interferometric synthetic-aperture radar data using deep learning. *Scientific Reports*, 11(1), 1-10.

Milillo, P., Rignot, E., Rizzoli, P., Scheuchl, B., Mouginot, J., Bueso-Bello, J. L., ... & Dini, L. (2022). Rapid glacier retreat rates observed in West Antarctica. *Nature Geoscience*, 15(1), 48-53.

Brancato, V., Rignot, E., Milillo, P., Morlighem, M., Mouginot, J., An, L., ... & Prats-Iraola, P. (2020). Grounding line retreat of Denman Glacier, East Antarctica, measured with COSMO-SkyMed radar interferometry data. *Geophysical Research Letters*, 47(7).

Milillo, P., Rignot, E., Rizzoli, P., Scheuchl, B., Mouginot, J., Bueso-Bello, J., & Prats-Iraola, P. (2019). Heterogeneous retreat and ice melt of Thwaites Glacier, West Antarctica. *Science Advances*, 5(1).

Milillo, P., Rignot, E., Mouginot, J., Scheuchl, B., Morlighem, M., Li, X., & Salzer, J. T. (2017). On the short-term grounding zone dynamics of Pine Island Glacier, West Antarctica, observed with COSMO-SkyMed interferometric data. *Geophysical Research Letters*, 44(20), 10-436.

Scheuchl, B., Mouginot, J., Rignot, E., Morlighem, M., & Khazendar, A. (2016). Grounding line retreat of Pope, Smith, and Kohler Glaciers, West Antarctica, measured with Sentinel-1a radar interferometry data. *Geophysical Research Letters*, 43(16), 8572-8579.

Rignot, E., Mouginot, J., Morlighem, M., Seroussi, H., & Scheuchl, B. (2014). Widespread, rapid grounding line retreat of Pine Island, Thwaites, Smith, and Kohler glaciers, West Antarctica, from 1992 to 2011. *Geophysical Research Letters*, 41(10), 3502-3509.

Li, X., Rignot, E., Morlighem, M., Mouginot, J., & Scheuchl, B. (2015). Grounding line retreat of Totten Glacier, east Antarctica, 1996 to 2013. *Geophysical Research Letters*, 42(19), 8049-8056.

Rignot, E., Mouginot, J., & Scheuchl, B. (2011). Antarctic grounding line mapping from differential satellite radar interferometry. *Geophysical Research Letters*, 38(10).

6 DOCUMENT INFORMATION

6.1 Publication Date

January 2023

6.2 Date Last Updated

January 2023